MRS Advances (2024) 9:433–438
https://doi.org/10.1557/s43580-024-00792-6

ORIGINAL PAPER

Optimisation of synthesis procedures and structural investigation of monazite-cheralite solid solutions

Theresa Lender[1] · Luiza Braga Ferreira dos Santos[2] · Robert Gericke[2] · Nina Huittinen[2,3] · Lars Peters[1]

Received: 15 December 2023 / Accepted: 27 January 2024 / Published online: 14 February 2024

Abstract

The monazite-cheralite solid solutions LnPO$_4$-Ca$_{0.5}$Th$_{0.5}$PO$_4$ with Ln = La, Gd were prepared via a co-precipitation route, showcasing an optimised, scalable synthesis procedure for a possible waste form accommodating high level liquid waste streams. A distortion of the cheralite structure with respect to the monazite structure was observed throughout both solid solutions as evidenced by a deviation of the lattice parameters from the linear behaviour known from other monazite solid solutions. Using a high temperature flux method, cheralite single crystals were grown for the first time for in-depth structural investigations. Both thorium and calcium were found to deviate from the central position of the LnO$_9$ polyhedron, supporting previous neutron diffraction investigations of identical cheralite samples.

Introduction

The name-giving mineral cheralite (CaTh(PO$_4$)$_2$, formerly known as brabantite) is a naturally occurring mineral that has first been described by Rose [1]. It belongs to the monazite group and is formed by complete substitution of the rare-earth elements in LnPO$_4$ (Ln = La-Gd) with Ca^{2+} and Th^{4+} *via* the substitution mechanism:

$$2[Ln^{3+}PO_4] + Ca^{2+} + Th^{4+} \rightleftarrows [Ca^{2+}Th^{4+}(PO_4)_2] + 2Ln^{3+}.$$

Cheralite-type materials with other divalent cations, e.g. CdTh(PO$_4$)$_2$, SrTh(PO$_4$)$_2$ and PbTh(PO$_4$)$_2$ have been reported [2]. Phosphates with the monazite structure have been proposed as suitable waste forms for the conditioning of actinide-rich waste streams based on a number of advantageous characteristics including high chemical flexibility, low critical temperatures, high leaching stability, and favourable sintering properties (*e.g.* Schlenz et al. [3]). Natural cheralite minerals that have been able to withstand self-irradiation for millions of years, demonstrating their exceptional radiation tolerance [4].

The monazite structure is composed of alternating edge-sharing LnO$_9$ polyhedra and PO$_4$ tetrahedra forming infinite chains along the [001] direction. The polyhedra can be described as an equatorial pentagon formed by five oxygen atoms, interpenetrated by a tetrahedron constituted by four oxygen atoms which are part of the PO$_4$ tetrahedra [5]. Monazite crystallises in the monoclinic space group P2$_1$/n.

Several authors have described the synthesis of monazite-cheralite solid solutions. While a few studies have been published about different hydrothermal syntheses of monazite-cheralite solid solutions [6, 7] the most widely used method in literature is a solid state reaction (*e.g.* [8–11]). To our knowledge, only Montel et al. [2] have made use of a precipitation method for the synthesis of cheralite so far.

In this study, two monazite-cheralite solid solutions were prepared *via* a co-precipitation route involving a rhabdophane precursor, which is especially suited for aqueous, actinide-rich waste streams. In contrast to solid state methods, this synthesis route mostly avoids the use of solids thus reducing possibilities for dust formation. Additionally, the temperatures required for the conversion of rhabdophane to monazite (500–800 °C, according to Jonasson et al. [12]) have been reported to be considerably lower than those needed for solid state synthesis (≥ 1200 °C) [8, 9] hence improving the feasibility for large-scale application.

✉ Theresa Lender
lender@ifk.rwth-aachen.de

[1] Institute of Crystallography, RWTH Aachen University, 52066 Aachen, Germany

[2] Institute of Resource Ecology, Helmholtz-Zentrum Dresden-Rossendorf, Bautzner Landstraße 400, Dresden, Germany

[3] Institute of Chemistry and Biochemistry, Freie Universität Berlin, Fabeckstraße 34-36, Berlin, Germany

Working at ambient pressure also facilitates future upscaling and reduces hazards connected to pressurized vessels.

Single crystals of cheralite were grown using a high temperature flux method. They were analysed with X-ray diffraction to investigate the structural distortion of cheralite with respect to monazite as described by Raison et al. [9]. Deviations from the ideal behaviour can have significant impact on the physicochemical properties of a solid solution and should therefore be studied in detail.

Materials and methods

Powder synthesis

Both monazite-cheralite solid solutions $La_{1-x}Ca_{x/2}Th_{x/2}PO_4$ and $Gd_{1-x}Ca_{x/2}Th_{x/2}PO_4$ were produced via a co-precipitation route following the literature protocol by Heuser et al. [13]. The respective metal nitrates were mixed with phosphoric acid and citric acid, which was used as a complexing agent. Commercial $La(NO_3)_3{\cdot}6H_2O$ (Merck, 99%), $Gd(NO_3)_3{\cdot}6H_2O$ (Sigma-Aldrich, 99.9%), $Ca(NO_3)_2$ (Alfa Aesar, 97%), $Th(NO_3)_4$ (Th-232), citric acid (Merck, 99%) and phosphoric acid (Sigma-Aldrich, 99,8%) were used in the synthesis. All nitrates were dried overnight at 90 °C. Precipitation of rhabdophane was induced by increasing the pH with 12.5 % ammonia solution. The precipitate was washed six times with ultrapure water. After a drying step, the powders were pre-calcined at 550 °C for 3 h and calcined at 1200 °C for 4 h under Ar atmosphere to remove crystal water and obtain monazite. The applied temperature is well below the decomposition temperature of cheralite, which was reported to be 1400 °C [8] and high enough to ensure complete and rapid phase conversion. All synthesis steps were performed in a glovebox.

Single crystal synthesis

Cheralite single crystals were synthesized by a high-temperature solution (flux) method as described by Cherniak et al. [14]. The molar ratio of the flux components was 75:25:2 ≡ MoO_3:Li_2CO_3:$Ca_{0.5}Th_{0.5}PO_4$ or $La_{0.5}Ca_{0.25}Th_{0.25}PO_4$ assuming the full conversion of CaO, La_2O_3, ThO_2 and $NH_4H_2PO_4$ to cheralite during single crystal growth. Commercial MoO_3 (Acros, 99.5%), Li_2CO_3 (Merck, 99%), CaO (Thermo Scientific, 99.95%), La_2O_3 (Alfa Aesar, 99.9%) and $NH_4H_2PO_4$ (Bernd Kraft, 99%) were used in the synthesis while ThO_2 was obtained by precipitation from the $Th(NO_3)_4$ (Th-232) stock solution using 12.5% ammonia solution. The precipitate was washed with Milli-Q water and calcined at 600 °C for 4 h. The homogeneity of the flux solution was ensured by holding it at 1350 °C for more than 12 h for complete dissolution of the metal oxides. Subsequent cooling to 870 °C with a cooling rate of 2 °C/h enabled single crystal growth. Afterwards, the solutions were removed from the furnace and cooled in air. The grown single crystals were extracted by dissolving the flux in water in an ultrasonic bath. All experiments were carried out in closed platinum crucibles.

XRD

Powder X-ray diffraction patterns were obtained with a Rigaku MiniFlex 600 diffractometer equipped with a one-dimensional Rigaku D/teX Ultra Si strip detector, using a Cu-tube and a Ni-filter at a tube voltage of 40 kV and a current of 15 mA. The measurements were performed at ambient temperatures in the 2θ-range of 5°–90°. Structure refinements were performed using the Rietveld-method [15] within the *Topas Academic* software (Version 7.20) [16]. During the refinements, a ten coefficient Chebyshev-polynomial was used to describe the background. Crystallite size, lattice parameters, and fractional coordinates of all sites were allowed to vary. To account for the lower scattering power of oxygen and phosphorous compared to lanthanides, soft distance restraints for the P – O bonds were implemented at a value of 1.52 Å. The $LaPO_4$ structure published by Hirsch et al. [17] was used as starting model for the structural refinement. It should be noted that the estimated standard deviations of refined parameters are systematically underestimated in Rietveld refinements due to local correlations [18].

Single crystals were placed in mineral oil, cut, mounted on a 100 μm MiTeGen Dual Thickness MicroMount and located in the temperature-controlled N_2 gas flow at 100 K from Oxford instruments. The data was collected on a Bruker D8 VENTURE diffractometer equipped with a Photon II 7 array detector and micro focus Mo Kα radiation (λ = 0.71073 Å) with mirror optics monochromator. The computer programs SMART [19] and SAINT [20] were used for data collection in ϕ- and ω-scan modes and data processing, respectively. Absorption correction was performed using SADABS [21]. All structures were solved using ShelXT [22] and all atoms were refined with a Gauss-Newton model in Olex2 v1.3-ac4 [23]. Due to the close spatial proximity, the thermal displacement parameters of lanthanum, calcium and thorium atoms were refined isotropically to reduce correlation effects.

Results and discussion

The synthesis of both solid solutions $La_{1-x}Ca_{x/2}Th_{x/2}PO_4$ and $Gd_{1-x}Ca_{x/2}Th_{x/2}PO_4$ was successful over the complete range of substitutions as shown in Figure 1. Rietveld analysis confirmed the monazite structure in all samples. Powders with a substitution level of $x \geq 0.5$ of both solid solutions were

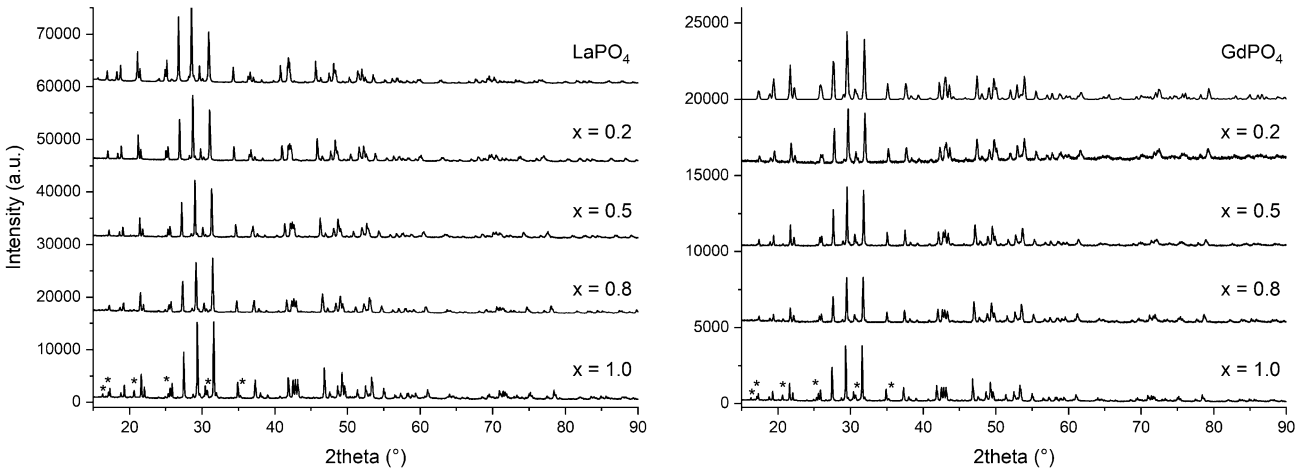

Fig. 1 Powder diffractograms of the solid solutions of $Ca_{0.5}Th_{0.5}PO_4$ with $LaPO_4$ (left) and $GdPO_4$ (right). Reflections originating from β-TPD are marked in the cheralite diffractogram

found to contain minute amounts of thorium phosphate-diphosphate $Th_4(PO_4)_4P_2O_7$ (β-TPD), which itself has been proposed as a waste matrix due to its resistance to aqueous corrosion [24].

The evolution of the lattice parameters within the solid solutions is displayed in Fig. 2a for $La_{1-x}Ca_{x/2}Th_{x/2}PO_4$ and Fig. 2b for $Gd_{1-x}Ca_{x/2}Th_{x/2}PO_4$. The unit cell parameters of both solid solutions vary almost linearly according to Vegard's law resulting in a small excess volume ($V_E/V_{Vegard} < 0.3$ %, compare Table I in the SI). The excess volume is an indicator for non-ideal mixing of the cations due to different oxidation states and ionic radii. Excess volumes of similar magnitude have been reported by Konings et al. [10] for the solid solutions $LnPO_4$-$Ca_{0.5}Th_{0.5}PO_4$ with Ln = La and Ce.

No significant differences can be observed between the evolution of lattice parameters in this study and other studies

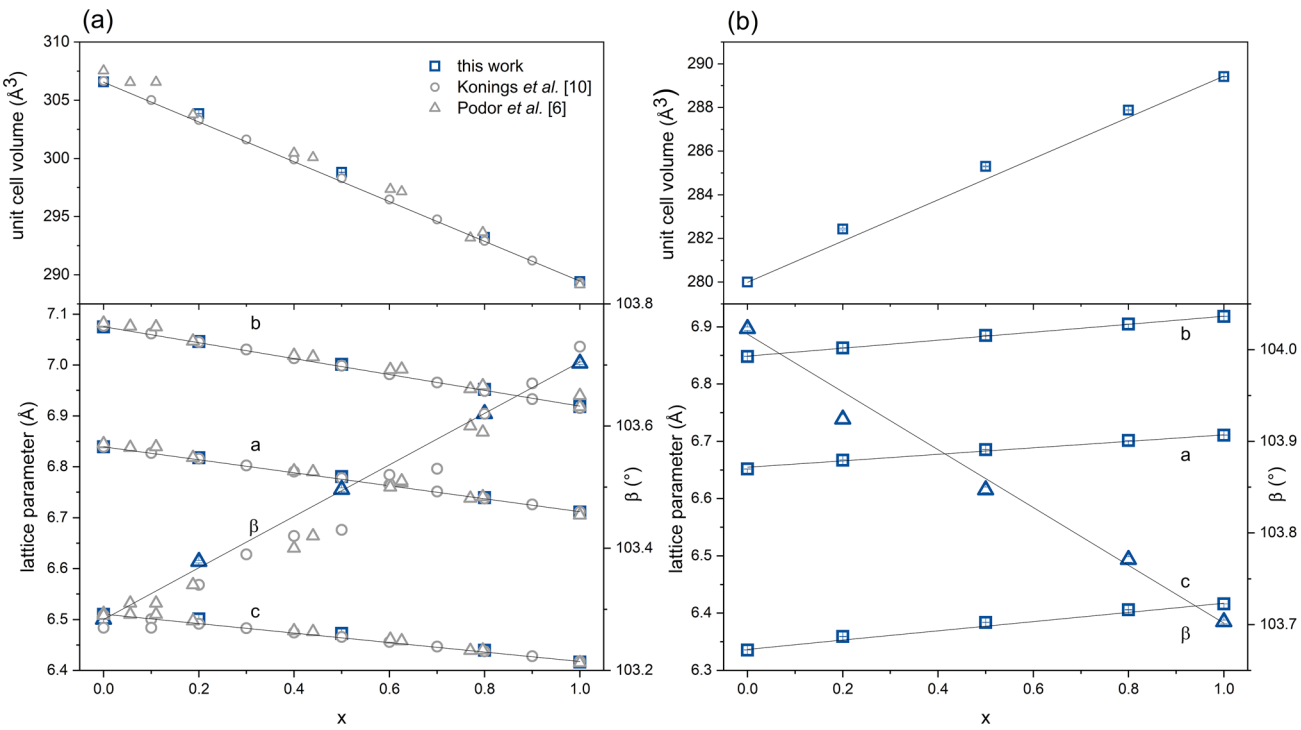

Fig. 2 Evolution of the lattice parameters of the solid solutions of $Ca_{0.5}Th_{0.5}PO_4$ with **a** $LaPO_4$ and **b** $GdPO_4$. Unit cell parameters change almost linearly and agree well with data published from different synthesis routes. Error bars are smaller than the symbols used

using hydrothermal [6] and solid state methods [10] apart from somewhat larger values for the monoclinic angle β. This highlights the equivalence of the synthesis procedures with respect to the product quality.

In available literature, it has been established that the lattice parameters of monazite compounds containing any two *Ln*(III) cations (La-Gd) change linearly with the average effective ionic radius [25]. This behaviour is not reproduced by the two newly synthesised solid solutions, as shown in Fig. 3. A deviation of the unit cell volume of cheralite from this linear relationship has first been described by Raison et al. [9], who attributed this observation to distortions in the PO_4 tetrahedra, despite the general finding that the tetrahedra are intrinsically more rigid in the monazite structure than the LnO_9 polyhedra [26]. In a subsequent publication, Raison et al. [27] revoked this conclusion based on neutron diffraction measurements. These indicated a small displacement of the calcium and thorium atoms from the central position of the LnO_9 polyhedron, thus imitating a cation with a radius of 1.29 Å rather than the average effective ionic radius of 1.135 Å calculated from the ionic radii given in Shannon [28].

Single crystal structure refinements on crystals of the compositions $Ca_{0.5}Th_{0.5}PO_4$ and $La_{0.5}Ca_{0.25}Th_{0.25}PO_4$ confirm the observations made by Raison et al. [27] (see Table II in the SI for refinement parameters). The distances between the cation positions were found to be $d_{Th\text{-}Ca}$ = 0.204(7) Å in $Ca_{0.5}Th_{0.5}PO_4$ and $d_{Th\text{-}Ca}$ = 0.160(14) Å, $d_{La\text{-}Ca}$ = 0.198(14) Å and $d_{La\text{-}Th}$ = 0.127(5) Å in $La_{0.5}Ca_{0.25}Th_{0.25}PO_4$. As described by Raison et al. [27], the thorium ions occupy a position closer to the centre of the polyhedron compared to calcium as evidenced by the more homogeneous bond length distribution (2.337(8)-2.863(8) Å for Th-O vs 2.412(10)-3.065(10) Å for Ca-O, see Table 1). In the case of $La_{0.5}Ca_{0.25}Th_{0.25}PO_4$, the La-O-bonds show the smallest spread (2.339(5)-2.830(5) Å) followed by Th-O (2.374(5)-2.943(6) Å) and Ca-O (2.384(10)-3.003(14) Å). It is interesting to note that the La-O bond distance distribution is still significantly larger than that in the $LaPO_4$ structure (2.459(8)-2.827(8) Å, [17]). This, however, is biased by the spatial averaging of the environment of Th, La, and Ca, respectively: In the final refinement, for each oxygen position one set of fractional coordinates (*x, y, z*) was refined, which is probably not an adequate description of the local, disordered situation. However, no significant distortion of the PO_4 tetrahedra was observed in any of the refinements. A tilt of the tetrahedra with respect to the polyhedra in dependence of the central cation was checked for in corresponding refinements allowing for 2 (or 3, respectively) sets of fractional coordinates for each oxygen position, but could not be confirmed by the results. Hence, some of the local features of the La/Th/Ca-environment most likely were lost in the spatially averaging diffraction experiment.

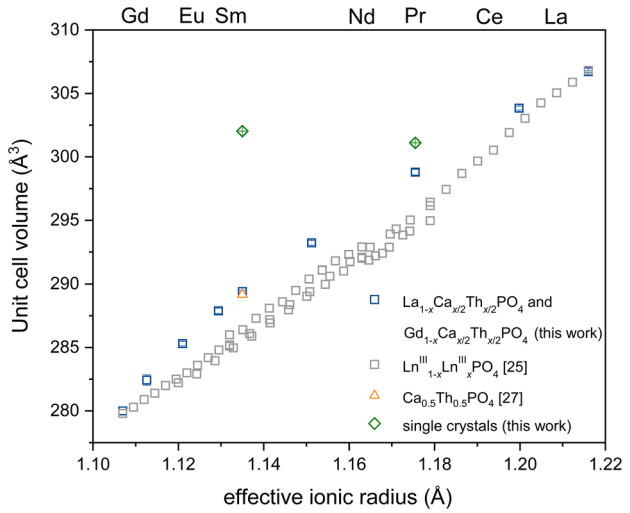

Fig. 3 Evolution of the unit cell parameters of monazite solid solutions as a function of their effective ionic radius according to Shannon [28]. The cheralite solid solutions deviate from the linear behaviour of the solid solutions containing only trivalent *Ln*

One major difference between the structural models obtained from powder samples and single crystals is the evolution of the lattice parameters. Both single crystal refinements result in larger unit cell volumes than observed in powder samples, including powders synthesised in this study and literature data [6, 10, 27] (see Fig. 3). This is counterintuitive, since the single crystals were measured at a lower temperature (100 K) compared to powder X-ray diffraction (ambient). Moreover, the surface to volume ratio is generally higher in powder samples, rather giving rise to the expectation of slightly larger unit cells for powder over single crystal data. A notable difference, however, was the sample preparation: The single crystals were obtained at high temperature (up to 1350 °C; powder: 1200 °C) over longer periods of time (18 days; powder: 7 h). Thus, a higher entropic contribution due to less statistically ordered occupation at the Ca/Th position in the single crystals over the powder sample is conceivable [30]. Furthermore, it cannot be ruled out that the deviation originates in part from the fact that the determination of lattice parameters from single crystals is less precise than from powders. As no chemical analysis of the single crystals was undertaken, we cannot exclude an influence of a hypothetical incorporation of the flux material, e.g. $Mo^{6+}O_4$ tetrahedra. This, however, has never been reported for flux-grown monazite single crystals containing trivalent lanthanides or actinides. Hence, the discrepancy in the lattice parameters needs to be resolved in a future study.

Table 1 Atomic distances and angles in $Ca_{0.5}Th_{0.5}PO_4$ and $La_{0.5}Ca_{0.25}Th_{0.25}PO_4$

Atoms	Distances (Å) in $Ca_{0.5}Th_{0.5}PO_4$	Distances (Å) in $La_{0.5}Ca_{0.25}Th_{0.25}PO_4$
Ca/Th/La-O1	3.065(10)/2.863(8)	3.003(14)/2.943(6)/2.830(5)
Ca/Th/La-O1'	2.461(11)/2.580(8)	2.575(14)/2.505(5)/2.600(5)
Ca/Th/La-O2	2.731(11)/2.604(9)	2.772(15)/2.631(7)/2.590(6)
Ca/Th/La-O2'	2.413(10)/2.448(8)	2.528(13)/2.402(5)/2.470(5)
Ca/Th/La-O2"	2.412(10)/2.337(8)	2.384(10)/2.374(5)/2.339(5)
Ca/Th/La-O3	2.503(10)/2.658(8)	2.481(14)/2.613(6)/2.674(5)
Ca/Th/La-O3'	2.529(11)/2.451(8)	2.390(15)/2.511(5)/2.428(6)
Ca/Th/La-O4	2.507(12)/2.667(9)	2.541(14)/2.600(7)/2.692(6)
Ca/Th/La-O4'	2.510(10)/2.527(7)	2.490(10)/2.533(5)/2.525(5)
P-O1	1.562(9)	1.560(5)
P-O2	1.576(9)	1.572(5)
P-O3	1.521(9)	1.508(5)
P-O4	1.555(8)	1.550(4)
O–P–O angles/O–O distances		
O1-P-O2/O1-O2	102.1(5)°/2.441(11)	102.2(3)°/2.438(6)
O1-P-O3/O1-O3	113.5(5)°/2.578(12)	113.7(3)°/2.569(7)
O1-P-O4/O1-O4	111.3(5)°/2.574(11)	111.4(3)°/2.568(6)
O2-P-O3/O2-O3	115.7(5)°/2.622(12)	115.3(3)°/2.602(6)
O2-P-O4/O2-O4	115.1(5)°/2.641(11)	115.4(3)°/2.639(6)
O3-P-O4/O3-O4	99.6(5)°/2.350(10)	99.3(3)°/2.330(6)

The designation of the oxygen atoms follows the structural model published by Ni et al. [29]

Conclusion

The present study demonstrates the chemical flexibility of the $La_{1-x}Ca_{x/2}Th_{x/2}PO_4$ and $Gd_{1-x}Ca_{x/2}Th_{x/2}PO_4$ monazite-cheralite system, achieving full solid solutions with both $LaPO_4$ and $GdPO_4$ endmembers, representing the largest and smallest lanthanides to form thermodynamically stable monazite. A previously reported structural deviation between cheralite and monazite evolves linearly with increasing substitution levels. The successful synthesis through a co-precipitation route presents a promising path for a scalable high-level waste conditioning process that reduces hazards arising from dust formation or pressurised reactions. To our knowledge, cheralite single crystals have been grown for the first time using a high temperature flux method, enabling us to study the atomic positions in the cheralite structure more precisely. We were able to confirm the conclusions drawn by Raison et al. [27] regarding the displacement of thorium and calcium ions from the central position in the LnO_9 polyhedron using standard laboratory XRD measurements.

Supplementary Information The online version contains supplementary material available at https://doi.org/10.1557/s43580-024-00792-6.

Author contributions Theresa Lender, Nina Huittinen and Lars Peters contributed to the study conception and design. Material preparation was performed by Theresa Lender and Luiza Braga Ferreira dos Santos, data collection and analysis were performed by Robert Gericke, Theresa Lender and Lars Peters. The first draft of the manuscript was written by Theresa Lender and all authors commented on previous versions of the manuscript. All authors read and approved the final manuscript.

Funding Open Access funding enabled and organized by Projekt DEAL. The authors thank the German Federal Ministry of Education and Research (BMBF) for funding under the project 02NUK060. This research was funded in part by the German Federal Ministry of Environment, Nature Conservation, Nuclear Safety and Consumer Protection (BMUV) under the project 1501667 (Am-BALL).

Data availability The authors declare that the data supporting the findings of this study are available within the paper and its Supplementary Information files. The single crystal structures have been submitted to the ICSD with the deposition numbers 2313937 and 2,313,938 for $La_{0.5}Ca_{0.25}Th_{0.25}PO_4$ and $Ca_{0.5}Th_{0.5}PO_4$, respectively. Should any raw data files be needed in another format they are available from the corresponding author upon reasonable request. Source data are provided with this paper.

Declarations

Competing interests On behalf of all authors, the corresponding author states that there is no conflict of interest.

References

1. D. Rose, Neues Jahrb. Mineral. Mh. **6**, 247 (1980)
2. J.-M. Montel, J.-L. Devidal, D. Avignant, Chem. Geol. (2002). https://doi.org/10.1016/S0009-2541(02)00150-X
3. H. Schlenz, J. Heuser, A. Neumann et al., Z Kristallogr Cryst Mater (2013). https://doi.org/10.1524/zkri.2013.1597
4. A. Guastoni, C. Mazzoli, Mitt. Österr. Mineral. Ges. **153**, 279 (2007)
5. N. Clavier, R. Podor, N. Dacheux, J. Eur. Ceram. Soc. (2011). https://doi.org/10.1016/j.jeurceramsoc.2010.12.019
6. R. Podor, M. Cuney, Am. Mineral. (1997). https://doi.org/10.2138/am-1997-7-815
7. D. Qin, A. Mesbah, N. Clavier et al., Cryst. Growth Des. (2019). https://doi.org/10.1021/acs.cgd.9b00028
8. D. Bregiroux, O. Terra, F. Audubert et al., Inorg. Chem. (2007). https://doi.org/10.1021/ic7012123
9. P.E. Raison, R. Jardin, D. Bouëxière et al., Phys. Chem. Miner. (2008). https://doi.org/10.1007/s00269-008-0252-4
10. R. Konings, M. Walter, K. Popa, J. Chem. Thermodyn. (2008). https://doi.org/10.1016/j.jct.2008.03.009
11. K. Popa, D. Bregiroux, R.J. Konings et al., J. Solid State Chem. (2007). https://doi.org/10.1016/j.jssc.2007.06.006
12. R. Jonasson, E. Vance, Thermochim. Acta (1986). https://doi.org/10.1016/0040-6031(86)85078-X
13. J.M. Heuser, S. Neumeier, L. Peters et al., J. Solid State Chem. (2019). https://doi.org/10.1016/j.jssc.2019.02.028
14. D. Cherniak, J. Pyle, J. Rakovan, Am. Mineral. (2004). https://doi.org/10.2138/am-2004-1023
15. H.M. Rietveld, Acta Cryst. (1967). https://doi.org/10.1107/S0365110X67000234
16. R.W. Cheary, A. Coelho, J. Appl. Crystallogr. (1992). https://doi.org/10.1107/S0021889891010804
17. A. Hirsch, P. Kegler, I. Alencar et al., J. Solid State Chem. (2017). https://doi.org/10.1016/j.jssc.2016.09.032
18. H.G. Scott, J. Appl. Crystallogr. (1983). https://doi.org/10.1107/S0021889883010195
19. W. Bruker AXS Inc.: Madison, Smart software ver. 5.625 for the ccd detector system (2001)
20. W. Bruker AXS Inc.: Madison, Saintplus software ver. 6.22 for the ccd detector system (2001)
21. R.H. Blessing, Acta Cryst. (1995). https://doi.org/10.1107/S0108767394005726
22. G. M. Sheldrick, Shelxtl, ver. 2013/4 (2013)
23. O.V. Dolomanov, L.J. Bourhis, R.J. Gildea et al., J. Appl. Crystallogr. (2009). https://doi.org/10.1107/S0021889808042726
24. N. Dacheux, B. Chassigneux, V. Brandel et al., Chem. Mater. (2002). https://doi.org/10.1021/cm011277g
25. A. Hirsch, Dissertation (2018) https://doi.org/10.18154/RWTH-2018-225331
26. M.M. Zaman, S.M. Antao, Minerals (2020). https://doi.org/10.3390/min10111028
27. P.E. Raison, S. Heathman, G. Wallez et al., Phys Chem Minerals (2012). https://doi.org/10.1007/s00269-012-0522-z
28. R.D. Shannon, Acta Cryst. (1976). https://doi.org/10.1107/S0567739476001551
29. Y. Ni, J.M. Hughes, A.N. Mariano, Am. Mineral. (1995). https://doi.org/10.2138/am-1995-1-203
30. T.J.B. Holland, Am. Mineral. **47**, 5–13 (1989)